npj Parkinson's Disease

https://doi.org/10.1038/s41531-025-01257-9

Article in Press

Alterations of cerebrospinal fluid flow dynamics in Parkinson's disease

Received: 31 October 2025

Accepted: 31 December 2025

Cite this article as: Zhou, C., Hong, H., Chen, Y. *et al.* Alterations of cerebrospinal fluid flow dynamics in Parkinson's disease. *npj Parkinsons Dis.* (2026). https://doi.org/10.1038/s41531-025-01257-9

Cheng Zhou, Hui Hong, Yutong Chen, Xiaojun Guan, Tao Guo, Xiaojun Xu & Minming Zhang

Title page

Alterations of cerebrospinal fluid flow dynamics in Parkinson's disease

Cheng Zhou [1#], Hui Hong [1,2#], Yutong Chen [2#], Xiaojun Guan [1], Tao Guo [1], Xiaojun Xu[1], Minming Zhang [1*]

[1]Department of Radiology, The Second Affiliated Hospital, Zhejiang University School of Medicine, Hangzhou, China
[2]Department of Clinical Neurosciences, University of Cambridge, Cambridge, UK

[#] These authors contributed equally to this work.

*** Corresponding to:** Minming Zhang, Department of Radiology, The Second Affiliated Hospital, Zhejiang University School of Medicine, No. 88 Jiefang Road, Shangcheng District, Hangzhou 310009, China. E-mail: zhangminming@zju.edu.cn.

Total word count: 3990

References: 51

Figures: 3

Tables: 2

Running title: Cerebrospinal Fluid Flow Dynamics in PD.

Abstract

Cerebrospinal fluid (CSF) flow dynamics play a critical role in clearing pathological proteins from the brain, which may potentially influence the progression of neurodegenerative diseases. We aimed to investigate the alterations of CSF flow dynamics in patients with Parkinson's disease (PD). We employed the multiple low b-values diffusion magnetic resonance imaging combined with CSF-based spatial statistics to evaluate changes of CSF pseudo-diffusivity within ventricles, sulci, and cisterns in PD. We assessed the relationships between CSF pseudo-diffusivity and other indirect markers of glymphatic system, including the diffusion-tensor imaging along the perivascular space (DTI-ALPS) index, the volume of the choroid plexus and perivascular spaces. We explored the association between CSF pseudo-diffusivity and the integrity of the locus coeruleus (LC). A total of 44 patients and 48 healthy controls participated in the study. PD patients showed significantly reduced CSF pseudo-diffusivity within the ventricles and sulci, with no significant changes within the cisterns. Lower CSF pseudo-diffusivity was correlated with lower DTI-ALPS index. Furthermore, decreased CSF pseudo-diffusivity was correlated with LC degeneration. These findings suggested that PD exhibit reduced CSF flow dynamics within the ventricles and sulci. Furthermore, LC-norepinephrine system dysfunction may represent a potential mechanism and target for modulating CSF flow dynamics.

Keywords: Parkinson's disease, Cerebrospinal fluid, Diffusion Weighted Imaging, Glymphatic system, Locus coeruleus.

Introduction

Parkinson's disease (PD) is a neurodegenerative disorder characterized by the accumulation of misfolded alpha-synuclein protein in regions such as the substantia nigra[1]. Currently, there are no effective methods to clear or slow the progressive deposition of the misfolded α-synuclein protein[2]. The glymphatic system is a pathway that allows cerebrospinal fluid (CSF) to flow in and interstitial fluid (ISF) to flow out through the perivascular space (PVS)[3-6]. This system facilitates the clearance of waste products and pathological proteins, such as amyloid-beta and α-synuclein[7-9]. Most studies on the glymphatic system have primarily focused on the structure of PVS and the outflow of ISF[6,10,11]. However, the inflow of CSF, which acts as the main driving force for fluid exchange within the glymphatic system, has received comparatively less attention[12-14]. Elucidating the alterations of the inflow of CSF in PD may offer novel insights into the pathological mechanisms and potential intervention strategies.

CSF is produced by the choroid plexus and flows through the ventricles, cisterns, and sulci of the brain. Animal studies have shown a close relationship between CSF flow dynamics and the metabolism of pathological substances[14,15]. A recent study reported that norepinephrine oscillations during sleep can regulate vascular and CSF flow, thereby modulating glymphatic clearance efficiency. And pharmacological inhibition of vascular and CSF motion reduces glymphatic clearance in mice[16]. PD mice model study have suggested that 40 Hz light stimulation can enhance the CSF flow, and combined auditory and visual stimulation reduces neuronal α-synuclein deposition in mice and alleviates both motor and non-motor symptoms in PD mice[8,17]. These studies suggested that improving CSF flow may contribute to clearing PD pathology, making it a highly promising therapeutic target. However, these findings still need to be confirmed in PD patients in vivo.

The traditional method for measuring the CSF flow dynamics is contrast-enhanced MRI, which involves injecting contrast agents into the CSF[18]. Nevertheless, the invasive nature of this method, coupled with the drawbacks of potential contrast agent allergies and long-term brain damage, restricts its widespread use. Recently, low b-value diffusion magnetic resonance imaging (low-b dMRI) has been reported to be useful in the observation of CSF flow in vivo[19,20]. Low-b dMRI is highly sensitive to a broad spectrum of incoherent motion, ranging from 0.1 to 1000 × 10^{-3} mm^2/s, which is referred to as pseudo-diffusivity. It is capable of detecting the fluctuations in

the pseudo-diffusivity of CSF diffusion at a microscopic scale[20,21]. A recent study firstly detected reduced CSF motion at the level of the suprasellar cistern in participants with versus without PD[22]. However, there is a significant variation in CSF motion across different regions. The closer to the large vessels at the base of the skull, the faster the CSF motion[19]. Therefore, the CSF motion within the suprasellar cistern may not represent the state of the CSF flow, and an evaluation of the CSF motion within different anatomical regions is needed.

Our recent study introduced a novel technique, CSF-based spatial statistics (CBSS), to automatically quantify CSF pseudo-diffusivity within different areas, including the ventricles, cisterns, and sulci[21]. This method overcomes the challenges posed by the significant individual variation in the anatomy of the CSF-filled sulci, cisterns, and ventricles, as well as the strong subjectivity associated with manual delineation of regions of interest. On the basis of this method, this study aimed to verify whether there are abnormalities in the CSF flow dynamics in PD patients. We further assessed the relationship between CSF flow and other indirect MRI measures employed to assess glymphatic system function, including diffusion-tensor imaging analysis along the perivascular space analysis (DTI-ALPS), volume of choroid plexus and PVS. Lastly, given that the locus coeruleus (LC) serves as the primary source of norepinephrine in the brain, we evaluated the relationship between CSF flow and the integrity of the LC.

Results

Demographic and clinical characteristics were shown in *Table 1*. PD patients showed significantly decreased CSF pseudo-diffusivity within the combined ventricles ($P < 0.001$) and sulci ($P = 0.001$), but not within the combined cisterns, when compared with healthy controls (*Figure 2*, FDR corrected). The differences in CSF pseudo-diffusivity within the subregions of the ventricles, sulci, and cisterns were described in Table 2 (FDR corrected).

No significant difference was found in DTI-ALPS index, choroid plexus volume, and PVS volume between two groups. We found that the CSF pseudo-diffusivity within both ventricles and cisterns were significantly correlated with the DTI-ALPS index in patient group ($r = 0.437$, $P < 0.001$, $r = 0.322$, $P = 0.003$, respectively, FDR corrected). The CSF pseudo-diffusivity within the sulci was not correlated with DTI-ALPS index.

Significant lower CNR_{LC} was found in PD patients when compared with healthy controls (P

= 0.044, *Figure 3A*). Additionally, CSF pseudo-diffusivity within the combined ventricles and sulci are significantly correlated with LC integrity (r = 0.454, P= 0.006, and r = 0.384, P= 0.013, respectively, *Figure 3 B, C*, FDR corrected) in patients. However, no significant correlation was found between CSF pseudo-diffusivity within the combined cisterns and LC degeneration.

Pearson correlation analysis showed that the CSF pseudo-diffusivity of the combined ventricles was significantly associated with tremor score and SCOPA-AUT score (r = -0.330, P = 0.029 and r = -0.342, P = 0.031, respectively, uncorrected). However, these associations no longer reached statistical significance after adjusting for the effects of age, sex, and the combined ventricular volume. No significant correlation was found between CSF pseudo-diffusivities and disease duration, LEDD, H&Y stage, UPDRS, four major motor symptoms, MMSE, and RBDQ-HK scores.

Discussion

In this study, we employed a novel method named CBSS to measure the CSF motion within the ventricles, cisterns, and sulci. Our findings revealed a significant reduction in CSF motion within the ventricles and sulci of patients with PD. The CSF motion was significantly correlated with the DTI-ALPS index, an approximating measure of glymphatic function. Finally, we found that abnormal CSF motion showed a significant association with LC degeneration.

We found significantly reduced CSF pseudo-diffusivity in PD patients in vivo. Driven by factors such as cerebral vascular pulsation, CSF enters the brain parenchyma through the PVS[15,23,24]. It facilitates the exchange of substances between CSF and ISF, helps remove metabolic waste and pathological proteins via the PVS, and ultimately transfers these waste and proteins to deep cervical lymph nodes and the peripheral lymphatic system[23,24]. There is growing evidence indicating abnormal CSF circulation in PD and other neurodegenerative disorders[25,26]. Mice study suggests that meningeal lymphatic drainage dysfunction aggravates alpha-synuclein pathology and exacerbates motor and memory deficits[5]. The sleep aid zolpidem suppresses norepinephrine oscillations and CSF flow, then slows ISF exchange, and reduces glymphatic function[16]. Non-invasive MRI techniques used to assess brain fluid circulation encompass phase-contrast MRI (including 4D flow imaging), the DTI-ALPS index, and the CBSS method. Some of these measures have provided valuable insights into brain fluid circulation in PD[22,27]. Phase-contrast

MRI reflects the directional, bulk transport of CSF driven primarily by cardiac and respiratory pulsation, whereas the DTI-ALPS index quantifies water molecule diffusion characteristics within PVS[28,29]. In contrast, low-b diffusion captures the diffusion-like, incoherent motility of CSF arising from multidirectional pulsation, mixing, and small-scale motion within the subarachnoid or ventricular spaces[20,21]. In comparison with other methods, CBSS is more strongly affected by regional micro-environmental changes, such as local inflammation, impaired mixing, or waste accumulation that alter CSF micro-motility. Moreover, considering the substantial heterogeneity of CSF dynamics across different regions, CBSS could offer novel and complementary perspectives about CSF dynamics, which could enrich the understanding of CSF circulatory dysfunction in patients with PD. In this study, we further found that the reduction in CSF motion is evident in the ventricles and sulci, while CSF motion in the cisterns remains unaffected. Due to its close proximity to the blood vessels at the basis cranii, the cisterns, particularly the suprasellar cistern, are the region where CSF exhibits the greatest kinetic energy. As the energy in the cisterns dissipates during transmission to the surrounding sulci and ventricles, we hypothesize that abnormal CSF flow in PD may first manifest in regions with weaker kinetic energy like sulci and ventricles.

We found that lower CSF pseudo-diffusivity was significantly associated with lower DTI-ALPS index. Previous study has demonstrated a significant correlation between DTI-ALPS index and Glymphatic MRI after intrathecal administration of gadolinium[30]. Thus, the DTI-ALPS index has been widely used as an approximating measure of glymphatic function in vivo[31]. A lower DTI-ALPS index has been identified in PD and is associated with the clinical symptoms and prognosis of PD[27,32]. The correlation between the two MRI measures highlighted the clinical significance of CSF pseudo-diffusivity and suggests a potential association between CSF flow and the pathophysiological changes represented by the DTI-ALPS index. Moreover, we did not detect a significant reduction in the DTI-ALPS index in our PD cohort, suggesting that CSF pseudo-diffusivity may be a more sensitive measure of glymphatic dysfunction in PD. It is worth noting that while DTI-ALPS is widely interpreted as an indirect measure of glymphatic function, most recent study suggests this metric may be biased and confounded by white matter structural alterations, rather than directly reflecting neuro-fluid dynamics[33]. Therefore, the significance of this measure should be interpreted with caution.

Notably, we identified an association between abnormal CSF motion and LC degeneration, a

core pathological feature of PD[34]. Recent work has demonstrated that the release of norepinephrine during non-rapid eye movement sleep in mice drives changes in cerebral blood volume and CSF flow, promoting glymphatic clearance[16]. Norepinephrine-regulated vasomotion serves as the key driving force for brain fluid transport[15]. Given that LC-norepinephrine neurons are the primary source of central norepinephrine, LC degeneration may thus impair the regulatory capacity of intracranial vessels, in turn altering CSF flow dynamics[35]. To our knowledge, no prior research has linked LC degeneration to CSF dynamics in patients with PD. We first report the association between LC degeneration and reduced CSF motion in PD in vivo, which suggests that LC degeneration may serve as a potential factor influencing CSF flow—thereby providing valuable insights for future therapeutic interventions. However, it should be noted that the CSF flow measurement in this study was conducted under awake conditions, which may differ from the CSF flow during sleep[16]. Future studies are needed to investigate the relationship between LC-norepinephrine system degeneration and changes in CSF flow during sleep state. Furthermore, future investigations are warranted to extend these findings to other neurological disorders marked by LC degeneration like Alzheimer's disease—to explore the relationship between LC degeneration and CSF dynamics in these populations. Such work would help clarify whether a common mechanism underpins CSF circulatory dysfunction across distinct neurological conditions.

However, we did not observe significant correlation between CSF pseudo-diffusivity, disease duration, motor and cognitive performance, RBD symptom, and autonomic nervous function. A recent small-sample study also failed to report an association between CSF dynamics and clinical symptoms[22]. This may be due to the small sample size, clinical heterogeneity, or the possibility of a nonlinear relationship between CSF flow and clinical manifestations. Collectively, these findings suggested that while CSF pseudo-diffusivity holds certain value in detecting CSF dynamic abnormalities in PD, its utility for assessing disease severity remains to be validated. Future large-sample studies are warranted to further investigate the relationship between CSF flow and clinical manifestation in patients with PD.

This study has several limitations. The small sample size constrains the generalizability of our findings, and larger studies are needed to confirm our results. Pseudo-diffusivity captures local microscale CSF motion influenced by diverse physiological factors (cardiac/respiratory/vascular pulsatility, motion) and acts as an indirect, non-exclusive proxy for glymphatic inflow.

Consequently, caution is warranted when interpreting the current findings. Due to the unavailability of reverse phase encoding images in our data acquisition, we were unable to perform correction for susceptibility-induced distortions, which constitutes a limitation of the present study. Additionally, the relatively low resolution in z-axis used in low-b dMRI and NM-MRI may have introduced partial volume effects, necessitating cautious interpretation of the results.

In conclusion, this study provided novel evidence that patients with PD exhibit reduced CSF motion in the ventricles and sulci, with no significant alterations in cisterns. Furthermore, we revealed a significant correlation between LC degeneration and reduced CSF motion, suggesting that dysfunction of the LC-norepinephrine system may represent a potential mechanism and target for future interventional research.

Methods

Participants

PD patients were recruited from the Department of Neurology, the Second Affiliated Hospital of Zhejiang University School of Medicine and diagnosed by experienced neurologists according to the Movement Disorder Society Clinical Diagnostic Criteria for Parkinson's disease[36]. Well-matched healthy controls were recruited from the community. Patients with a history of brain tumors, stroke, vascular malformation, cerebral trauma, psychiatric disorders, non-central nervous system malignancies, sedative/hypnotic medication, substance abuse, or participation in other trials were not included. MRI data were visually inspected and images showing obvious artifacts were excluded. Finally, 44 PD and 48 healthy controls were included in this study.

The protocol, consent form, and other relevant documentation were approved by the ethics committee of the local hospital before the study commenced (C2020001212). The study was performed in accordance with the Declaration of Helsinki. Before enrollment, all patients provided their written informed consent.

Clinical assessments

The Unified Parkinson's Disease Rating Scale (UPDRS) was utilized to assess various domains: Part I was employed for mental examination, Part II for evaluating activity of daily living, and Part

III for motor examination. We then calculated four major motor symptoms from UPDRS: bradykinesia (items 23, 24, 25, and 26), rigidity (items 22), tremor (items 20 and 21), and axial symptoms (items 18, 19, 27, 28, 29, and 30). Hoehn & Yahr (H&Y) scale was utilized to assess disease severity. Levodopa equivalent daily dose (LEDD) was calculated using established conversion factors for all dopaminergic medications[37]. Global cognition was assessed using the Mini-Mental State Examination (MMSE). Sleep and autonomic nervous function were assessed using Rapid Eye Movement Sleep Behavior Disorder Questionnaire—Chinese University of Hong Kong version (RBDQ-HK) and Scales for Outcomes in Parkinson's Disease—Autonomic (SCOPA-AUT), respectively. Clinical assessments were conducted during OFF state (at least 12 hours after withholding PD medications).

Magnetic resonance imaging data acquisition

All participants were scanned on a 3.0T MRI scanner equipped with an eight-channel head coil (MR750; GE Healthcare, Milwaukee, USA). As it has been shown that CSF dynamics are influenced by circadian rhythms, all MR scans were conducted between 8:00 AM and 11:00 AM[38]. The T1-weighted structural MRI was acquired using the fast spoiled gradient-recalled sequence: echo time (TE) = 3.036 ms; repetition time (TR) = 7.336 ms; inversion time = 450 ms; flip angle (FA) = 11°; field of view (FOV) = 260 × 260 mm^2; matrix = 256 × 256; slice thickness = 1.2 mm; voxel size = 1*1*1.2 mm. Diffusion tensor imaging (DTI) was acquired using a spin echo-echo planar imaging sequence: TR = 8000 ms; TE = 80 ms; flip angle = 90 degrees; field of view = 256 × 256 mm^2; matrix = 128 × 128; slice thickness = 2 mm; voxel size = 2*2*2 mm. DTI were acquired from 30 gradient directions (b = 1000 s/mm^2), and included five acquisitions without diffusion weighting (b = 0). Low-b dMRI was acquired with b-values of 0, 10, 20, 30, 50, 70, 90, 110, 130, 150, 170, 200, 500, 800, 1000 and 1500 s/mm^2 with each b-value being acquired under 3 different gradient directions; TR = 3000 ms; TE = 75ms; field of view = 256 × 256 mm^2; matrix = 128 × 128; slice thickness = 4 mm; voxel size = 2*2*4 mm. Both DTI and low b-value dMRI scans were acquired under posterior-to-anterior phase encoding direction. Reverse phase encoding images were not acquired and distortion correction was not performed. Neuromelanin-sensitive MRI (NM-MRI) was acquired using a T1-weighted fast spin echo sequence: TE = 18.6 ms; TR = 600 ms; FA = 77°; FOV = 220 × 220 mm^2; matrix = 512 × 512; number of slices = 17 (axial); slice thickness = 3 mm; voxel size = 0.43*0.43*3 mm. Scanning coverage was set from the top of basal

ganglia to the bottom of the medulla oblongata. The acquisition plane was orthogonal to the brainstem.

Cerebrospinal fluid-based spatial statistics

Low-b dMRI and DTI data were preprocessed using FMRIB Software Library (FSL, http://www.fmrib.ox.ac.uk/fsl)[39] and MRtrix3 (http://www.mrtrix.org)[40]. The preprocessing steps included denoising and removal of Gibbs ringing artifacts, followed by eddy current and motion correction using eddy_correct. Reverse phase encoding images were not acquired and distortion correction was not performed. The maps of free water and free water corrected fractional anisotropy (cFA) were obtained from processed DTI images. Free water calculation was performed using the script provided by the MarkVCID project (https://markvcid.partners.org/markvcid2-protocols-resources). Briefly, a two-compartment model—comprising a free water compartment (isotropic tensor) and a tissue compartment (anisotropic tensor)—was fitted to the signal in each voxel. The free water map denotes the fractional volume (0–1 range) of the free water compartment. After calculation, the white matter fraction map was segmented from the cFA map using Atropos in Advanced Normalization Tools (ANTs, https://www.ants.dev/docs)[41]. The CSF fraction map was derived from the free water map with a threshold of free water fraction larger than 0.8. The gray matter (GM) fraction map was obtained by one minus the CSF and white matter fraction maps, which is similar to the gray matter-based spatial statistics[42]. The pseudo-T2 map was generated by mixing the maps corresponding to CSF and GM fractions in 2:1 ratio, as increased contrast in the CSF regions may increase the accuracy of CSF segmentation. Susceptibility-induced distortion can reduce the registration accuracy between dMRI and T1-weighted images. We circumvent this limitation by generating a pseudo-T2 image from dMRI data, thereby avoiding the need to register distorted (dMRI) and undistorted (T1) image modalities and improving overall registration precision. The CSF regions including ventricles and subarachnoid space were segmented by FreeSurfer SynthSeg (https://surfer.nmr.mgh.harvard.edu)[43]. Lateral, third and fourth ventricles were contained in the FreeSurfer segmentation. To parcellate the subarachnoid space into subregions, we registered the sulcus-specific GM atlas[21] to pseudo-T2 image in the native space using the symmetric normalization technique in ANTs. This GM atlas allowed for the parcellation of the subarachnoid space by using the nearest neighbor approach. Each voxel in the subarachnoid space was labeled based on the closest GM voxel in terms of Euclidean distance. Only voxels with

a free water fraction of 0.8 or larger were considered in the parcellation. The resulting CSF parcellation was warped to the low b-value dMRI images. The transform was obtained by rigidly registering the b0 volume of DTI data to the b0 volume of the low b-value dMRI image.

The apparent diffusion coefficient was calculated using the b-values smaller than or equal to 200 s/mm^2 in the low b-value dMRI image, as pseudo-diffusivity/intra-voxel incoherent motion effect appeared when b≤200 s/mm^2. The signal attenuation was thought to result from the pseudo-diffusion of CSF water molecules, which can be represented by a single-compartment isotropic diffusion model.

$$S(b) = S(0)\, e^{-bD*} \quad (1)$$

where S(b) or S(0) is the signal of a voxel at a particular b-value or b-value = 0 s/mm^2. D* is pseudo-diffusivity that equivalent to the apparent diffusion coefficient. To reduce the impact of outliers within a CSF region, the median pseudo-diffusivity in each CSF region was calculated, rather than mean pseudo-diffusivity. Pseudo-diffusivities were derived for a total of 29 regions, including 3 ventricles and 26 cisterns and sulci. The names of these regions are provided in the supplementary materials. Finally, the labels of all ventricles, cisterns, and sulci are merged respectively, and the pseudo-diffusivities of the combined ventricles, combined cisterns, and combined sulci are calculated. The detailed workflow of CBSS is shown in *Figure 1*. The source code for CBSS processing is provided in https://github.com/Yutong441/CBSS.

Diffusion-tensor imaging analysis along the perivascular space analysis

Preprocessed DTI data underwent skull stripping, and the FSL dtifit function generated FA map and tensor maps representing diffusivity in all three dimensions (x, y, and z) for each participant. All tensor maps were normalized to MNI space using FSL using the FA map. Based on the JHU-ICBM-DTI-81-whitematter Labeled Atlas, the projection and association fibers located at the level of the lateral ventricle body were identified as the superior corona radiata (SCR) and superior longitudinal fasciculus (SLF). Regions of interest (ROIs) were delineated as spherical regions with a 5mm diameter in the bilateral SCR and SLF areas. The central coordinates of these ROIs, referenced to the JHU-ICBM-FA template, were specified as follows: right SCR (64, 110, 99), right SLF (51, 110, 99), left SCR (116, 110, 99), and left SLF (128, 110, 99)[44]. We applied a mask with an FA threshold greater than 0.2 to exclude CSF voxels. The DTI-ALPS index is calculated as the ratio of the mean x-axis diffusivity in the projection fiber (Dxproj) and the x-axis diffusivity

in the association fiber (Dxassoc) to the mean y-axis diffusivity in the projection fiber (Dyproj) and the z-axis diffusivity in the association fiber (Dzassoc). The formula for the DTI-ALPS index is as follows:

$$DTI - ALPS\ index = \frac{mean\ (Dxproj, Dxassoc)}{mean\ (Dyproj, Dzassoc)} \quad (2)$$

To assess the potential impact on white matter integrity, we regressed the average fractional anisotropy and mean diffusivity for each subject's entire brain white matter, following the methodology established in previous study[45]. Detailed methods for calculating DTI-ALPS index were described in previous study[32,46].

Choroid plexus volume analysis

The choroid plexus is a multifunctional structure responsible for both the production of CSF and the formation of the blood-CSF barrier through the presence of tight junctions between choroidal epithelial cells. A recent study has unveiled an association between choroid plexus volume and glymphatic function[47], and subsequent research has employed choroid plexus volume as a noninvasive marker for the assessment of glymphatic function[48]. Volumetric analysis was performed automatically using the FreeSurfer. The total intracranial volume (TIV) and choroid plexus volume were determined.

Perivascular space volume analysis

PVS are fluid-filled compartments that encase cerebral blood vessels, facilitating the movement of fluids to and from the brain. Emerging research highlights the crucial function of PVS in transporting molecular debris from the brain into the CSF[49]. T1-weighted image was used for PVS segmentation. Perivascular space volume in deep white matter and basal ganglia was obtained using trained tensorflow models for the 3D Segmentation of Perivascular Spaces on either T1-Weighted Images with a 3D U-Shaped Neural Network[50].

Neuromelanin-sensitive MRI for evaluating locus coeruleus integrity

We used NM-MRI to measure the integrity of LC. Two authors, who were blinded to the subjects' information, performed twice manual measurements. These measurements were conducted using ITK-SNAP (https://sourceforge.net/projects/itk-snap). Detailed anatomical location for manual

measurements was described in our previous study[51]. The mean and standard deviation (SD) of the signal intensity (SI) in LC and pontine (PT) were calculated. The contrast to noise ratio of LC (CNR_{LC}) was calculated as (SI_{LC} – SI_{PT}) / SD_{PT}. The averaged CNR_{LC} value from twice assessments were used for final analysis. A lower CNR value indicates more serious degeneration.

Statistics

Descriptive statistics including frequencies and mean (SD) were used to describe demographic and clinical characteristics. General linear model (GLM) was conducted to evaluate the differences of CSF pseudo-diffusivity between PD patients and healthy controls, with age, sex, and CSF volume in each region as covariates. Group difference in DTI-ALPS index was analyzed using GLM, with age, sex, white matter FA and MD included as covariates. For group differences in PVS and choroid plexus volumes, age, sex, and TIV were incorporated as covariates. Group comparisons of the CNR_{LC} only adjusted for age and sex as covariates. Partial correlation analysis was conducted to assess the relationship between CSF pseudo-diffusivity, DTI-ALPS index, choroid plexus volume, PVS volume, LC integrity, and clinical characteristics, with age, sex, and CSF volume in each region as covariates. When conducting partial correlation analyses with the DTI-ALPS index, white matter FA and MD was additionally regressed out as covariates; whereas for correlation analyses with choroid plexus and PVS volume, TIV was regressed out instead. All statistical analyses were executed using SPSS V.25. Statistical significance was determined by a two-tailed P value < 0.05 for individual tests and a False Discovery Rates (FDR)-corrected P value < 0.05 for multiple comparison corrections.

Authors' contributions

M.Z. has full access to the data in the study and takes responsibility for the integrity of the data and the accuracy of the data analysis.

Concept and design: C.Z., H.H., and M.Z..

Acquisition, analysis, or interpretation of data: C.Z., X.G., T.G., and X.X..

Drafting of the manuscript: C.Z..

Critical review of the manuscript for important intellectual content: All authors.

Statistical analysis: C.Z., H.H., and Y.C..

Obtained funding: M.Z., C.Z., X.G., T.G., and X.X..

Administrative, technical, or material support: M.Z..

Supervision: M.Z..

Acknowledgements

We thank Shanghai Tengyun Biotechnology Co., Ltd. for developing Hiplot Pro platform (https://hiplot.com.cn/) and providing valuable tools for data analysis and visualization. Hiplot is a free tool and none of the authors have any financial interests or relationships to disclose that could inappropriately influence, or be perceived to influence, the work presented in this manuscript.

Code availability

The source code for CBSS processing is provided in https://github.com/Yutong441/CBSS.

Competing interests

The Authors declare no Competing Financial or Non-Financial Interests.

Data availability

The datasets generated during and/or analyzed during the current study are available from the corresponding author on reasonable request.

Funding

This work was supported by the National Natural Science Foundation of China (Grant Nos. 82302132, 82271935, 82171888, 82202091, 82001767, 91630314, 82071997, 82302136, 82202089, 82371906, 82302135, and 81971577), the Natural Science Foundation of Zhejiang Province (Grant No. LY22H180002, LQ21H180008, and Z24H180002), the 13th Five-year Plan for National Key Research and Development Program of China (Grant No. 2016YFC1306600), and the China Postdoctoral Science Foundation (2023M733085).

References

1 Bloem, B. R., Okun, M. S. & Klein, C. Parkinson's disease. *Lancet (London, England)* **397**, 2284-2303 (2021). https://doi.org:10.1016/s0140-6736(21)00218-x

2 Stocchi, F., Bravi, D., Emmi, A. & Antonini, A. Parkinson disease therapy: current strategies and future research priorities. *Nature reviews. Neurology* **20**, 695-707 (2024). https://doi.org:10.1038/s41582-024-01034-x

3 Yamamoto, E. A. *et al.* The perivascular space is a conduit for cerebrospinal fluid flow in humans: A proof-of-principle report. *Proceedings of the National Academy of Sciences of the United States of America* **121**, e2407246121 (2024). https://doi.org:10.1073/pnas.2407246121

4 Iliff, J. J. *et al.* A paravascular pathway facilitates CSF flow through the brain parenchyma and the clearance of interstitial solutes, including amyloid β. *Sci Transl Med* **4**, 147ra111 (2012). https://doi.org:10.1126/scitranslmed.3003748

5 Ding, X. B. *et al.* Impaired meningeal lymphatic drainage in patients with idiopathic Parkinson's disease. *Nature medicine* **27**, 411-418 (2021). https://doi.org:10.1038/s41591-020-01198-1

6 Klostranec, J. M. *et al.* Current Concepts in Intracranial Interstitial Fluid Transport and the Glymphatic System: Part I-Anatomy and Physiology. *Radiology* **301**, 502-514 (2021). https://doi.org:10.1148/radiol.2021202043

7 Zou, W. *et al.* Blocking meningeal lymphatic drainage aggravates Parkinson's disease-like pathology in mice overexpressing mutated α-synuclein. *Translational neurodegeneration* **8**, 7 (2019). https://doi.org:10.1186/s40035-019-0147-y

8 Liu, Y. *et al.* Non-invasive auditory and visual stimulation attenuates α-Synuclein deposition and improves motor and non-motor symptoms in PD mice. *Experimental neurology* **364**, 114396 (2023). https://doi.org:10.1016/j.expneurol.2023.114396

9 Drieu, A. *et al.* Parenchymal border macrophages regulate the flow dynamics of the cerebrospinal fluid. *Nature* **611**, 585-593 (2022). https://doi.org:10.1038/s41586-022-05397-3

10 Xue, X. *et al.* Aquaporin-4 deficiency reduces TGF-β1 in mouse midbrains and exacerbates pathology in experimental Parkinson's disease. *J Cell Mol Med* **23**, 2568-2582 (2019). https://doi.org:10.1111/jcmm.14147

11 Cui, H. *et al.* Decreased AQP4 Expression Aggravates α-Synuclein Pathology in Parkinson's Disease Mice, Possibly via Impaired Glymphatic Clearance. *J Mol Neurosci* **71**, 2500-2513 (2021). https://doi.org:10.1007/s12031-021-01836-4

12 Ryman, S. G. *et al.* Abnormal Cerebrovascular Activity, Perfusion, and Glymphatic Clearance in Lewy Body Diseases. *Movement disorders : official journal of the Movement Disorder Society* **39**, 1258-1268 (2024). https://doi.org:10.1002/mds.29867

13 Morawska, M. M. *et al.* Slow-wave sleep affects synucleinopathy and regulates proteostatic processes in mouse models of Parkinson's disease. *Sci Transl Med* **13**, eabe7099 (2021). https://doi.org:10.1126/scitranslmed.abe7099

14 McKnight, C. D., Rouleau, R. M., Donahue, M. J. & Claassen, D. O. The Regulation of Cerebral Spinal Fluid Flow and Its Relevance to the Glymphatic System. *Curr Neurol Neurosci Rep* **20**, 58 (2020). https://doi.org:10.1007/s11910-020-01077-9

15 Miyazaki, M. *et al.* Physical Exercise Alters Egress Pathways for Intrinsic CSF Outflow: An Investigation Performed with Spin-labeling MR Imaging. *Magnetic resonance in medical sciences : MRMS : an official journal of Japan Society of Magnetic Resonance in Medicine* **23**, 171-183 (2024). https://doi.org:10.2463/mrms.mp.2023-0005

16 Hauglund, N. L. *et al.* Norepinephrine-mediated slow vasomotion drives glymphatic clearance during

sleep. *Cell* (2025). https://doi.org:10.1016/j.cell.2024.11.027

17 Sun, X. *et al.* 40 Hz light flickering facilitates the glymphatic flow via adenosine signaling in mice. *Cell Discov* **10**, 81 (2024). https://doi.org:10.1038/s41421-024-00701-z

18 Ringstad, G. *et al.* Brain-wide glymphatic enhancement and clearance in humans assessed with MRI. *JCI Insight* **3** (2018). https://doi.org:10.1172/jci.insight.121537

19 Taoka, T. *et al.* Diffusion analysis of fluid dynamics with incremental strength of motion proving gradient (DANDYISM) to evaluate cerebrospinal fluid dynamics. *Jpn J Radiol* **39**, 315-323 (2021). https://doi.org:10.1007/s11604-020-01075-4

20 Bito, Y., Harada, K., Ochi, H. & Kudo, K. Low b-value diffusion tensor imaging for measuring pseudorandom flow of cerebrospinal fluid. *Magnetic resonance in medicine* **86**, 1369-1382 (2021). https://doi.org:10.1002/mrm.28806

21 Chen, Y., Hong, H., Nazeri, A., Markus, H. S. & Luo, X. Cerebrospinal fluid-based spatial statistics: towards quantitative analysis of cerebrospinal fluid pseudodiffusivity. *Fluids and barriers of the CNS* **21**, 59 (2024). https://doi.org:10.1186/s12987-024-00559-z

22 Pierobon Mays, G. *et al.* Reduced cerebrospinal fluid motion in patients with Parkinson's disease revealed by magnetic resonance imaging with low b-value diffusion weighted imaging. *Fluids and barriers of the CNS* **21**, 40 (2024). https://doi.org:10.1186/s12987-024-00542-8

23 Atchley, T. J., Vukic, B., Vukic, M. & Walters, B. C. Review of Cerebrospinal Fluid Physiology and Dynamics: A Call for Medical Education Reform. *Neurosurgery* **91**, 1-7 (2022). https://doi.org:10.1227/neu.0000000000002000

24 Wang, Y. *et al.* Cerebrovascular activity is a major factor in the cerebrospinal fluid flow dynamics. *Neuroimage* **258**, 119362 (2022). https://doi.org:10.1016/j.neuroimage.2022.119362

25 Rasmussen, M. K., Mestre, H. & Nedergaard, M. The glymphatic pathway in neurological disorders. *The Lancet. Neurology* **17**, 1016-1024 (2018). https://doi.org:10.1016/s1474-4422(18)30318-1

26 Tarasoff-Conway, J. M. *et al.* Clearance systems in the brain-implications for Alzheimer disease. *Nature reviews. Neurology* **11**, 457-470 (2015). https://doi.org:10.1038/nrneurol.2015.119

27 Ghaderi, S., Mohammadi, S., Jouzdani, A. F., Ahmadzadeh, A. M. & Fatehi, F. A systematic review and meta-analysis on glymphatic flow dysfunction in Parkinson's disease and Parkinsonism spectrum. *NPJ Parkinson's disease* **11**, 306 (2025). https://doi.org:10.1038/s41531-025-01151-4

28 Banta, A. R. *et al.* Quantification of Perivascular Flow Dynamics of Human Cerebrospinal Fluid Along Major Arteries Using Phase-Contrast MRI. *Radiology* **316**, e243521 (2025). https://doi.org:10.1148/radiol.243521

29 Williamson, N. H., Komlosh, M. E., Benjamini, D. & Basser, P. J. Limits to flow detection in phase contrast MRI. *J Magn Reson Open* **2-3** (2020). https://doi.org:10.1016/j.jmro.2020.100004

30 Zhang, W. *et al.* Glymphatic clearance function in patients with cerebral small vessel disease. *Neuroimage* **238**, 118257 (2021). https://doi.org:10.1016/j.neuroimage.2021.118257

31 Taoka, T. *et al.* Evaluation of glymphatic system activity with the diffusion MR technique: diffusion tensor image analysis along the perivascular space (DTI-ALPS) in Alzheimer's disease cases. *Jpn J Radiol* **35**, 172-178 (2017). https://doi.org:10.1007/s11604-017-0617-z

32 Zhou, C. *et al.* Glymphatic system dysfunction and risk of clinical milestones in patients with Parkinson disease. *Eur J Neurol* **31**, e16521 (2024). https://doi.org:10.1111/ene.16521

33 Schilling, K. G. *et al.* White Matter Geometry Confounds Diffusion Tensor Imaging Along Perivascular Space (DTI-ALPS) Measures. *Hum Brain Mapp* **46**, e70282 (2025). https://doi.org:10.1002/hbm.70282

34 Betts, M. J. *et al.* Locus coeruleus imaging as a biomarker for noradrenergic dysfunction in neurodegenerative diseases. *Brain* **142**, 2558-2571 (2019). https://doi.org:10.1093/brain/awz193

35 Knudsen, K. *et al.* In-vivo staging of pathology in REM sleep behaviour disorder: a multimodality imaging case-control study. *The Lancet. Neurology* **17**, 618-628 (2018).

https://doi.org:10.1016/s1474-4422(18)30162-5

36 Postuma, R. B. *et al.* MDS clinical diagnostic criteria for Parkinson's disease. *Movement disorders : official journal of the Movement Disorder Society* **30**, 1591-1601 (2015). https://doi.org:10.1002/mds.26424

37 Jost, S. T. *et al.* Levodopa Dose Equivalency in Parkinson's Disease: Updated Systematic Review and Proposals. *Movement disorders : official journal of the Movement Disorder Society* **38**, 1236-1252 (2023). https://doi.org:10.1002/mds.29410

38 Han, G. *et al.* Age- and time-of-day dependence of glymphatic function in the human brain measured via two diffusion MRI methods. *Frontiers in aging neuroscience* **15**, 1173221 (2023). https://doi.org:10.3389/fnagi.2023.1173221

39 Andersson, J. L. R. & Sotiropoulos, S. N. An integrated approach to correction for off-resonance effects and subject movement in diffusion MR imaging. *Neuroimage* **125**, 1063-1078 (2016). https://doi.org:10.1016/j.neuroimage.2015.10.019

40 Tournier, J. D. *et al.* MRtrix3: A fast, flexible and open software framework for medical image processing and visualisation. *Neuroimage* **202**, 116137 (2019). https://doi.org:10.1016/j.neuroimage.2019.116137

41 Avants, B. B., Tustison, N. J., Wu, J., Cook, P. A. & Gee, J. C. An open source multivariate framework for n-tissue segmentation with evaluation on public data. *Neuroinformatics* **9**, 381-400 (2011). https://doi.org:10.1007/s12021-011-9109-y

42 Vogt, N. M. *et al.* Cortical Microstructural Alterations in Mild Cognitive Impairment and Alzheimer's Disease Dementia. *Cerebral cortex (New York, N.Y. : 1991)* **30**, 2948-2960 (2020). https://doi.org:10.1093/cercor/bhz286

43 Billot, B. *et al.* Robust machine learning segmentation for large-scale analysis of heterogeneous clinical brain MRI datasets. *Proceedings of the National Academy of Sciences of the United States of America* **120**, e2216399120 (2023). https://doi.org:10.1073/pnas.2216399120

44 Liu, X. *et al.* Cross-Vendor Test-Retest Validation of Diffusion Tensor Image Analysis along the Perivascular Space (DTI-ALPS) for Evaluating Glymphatic System Function. *Aging Dis* **15**, 1885-1898 (2024). https://doi.org:10.14336/ad.2023.0321-2

45 Huang, S. Y. *et al.* Glymphatic system dysfunction predicts amyloid deposition, neurodegeneration, and clinical progression in Alzheimer's disease. *Alzheimer's & dementia : the journal of the Alzheimer's Association* **20**, 3251-3269 (2024). https://doi.org:10.1002/alz.13789

46 He, P. *et al.* The Association of the Glymphatic Function with Parkinson's Disease Symptoms: Neuroimaging Evidence from Longitudinal and Cross-Sectional Studies. *Ann Neurol* **94**, 672-683 (2023). https://doi.org:10.1002/ana.26729

47 Li, Y. *et al.* Choroid Plexus Enlargement Exacerbates White Matter Hyperintensity Growth through Glymphatic Impairment. *Ann Neurol* **94**, 182-195 (2023). https://doi.org:10.1002/ana.26648

48 Jeong, S. H. *et al.* Association of choroid plexus volume with motor symptoms and dopaminergic degeneration in Parkinson's disease. *Journal of neurology, neurosurgery, and psychiatry* **94**, 1047-1055 (2023). https://doi.org:10.1136/jnnp-2023-331170

49 Bown, C. W., Carare, R. O., Schrag, M. S. & Jefferson, A. L. Physiology and Clinical Relevance of Enlarged Perivascular Spaces in the Aging Brain. *Neurology* **98**, 107-117 (2022). https://doi.org:10.1212/wnl.0000000000013077

50 Boutinaud, P. *et al.* 3D Segmentation of Perivascular Spaces on T1-Weighted 3 Tesla MR Images With a Convolutional Autoencoder and a U-Shaped Neural Network. *Front Neuroinform* **15**, 641600 (2021). https://doi.org:10.3389/fninf.2021.641600

51 Zhou, C. *et al.* Locus coeruleus degeneration is associated with disorganized functional topology in Parkinson's disease. *NeuroImage. Clinical* **32**, 102873 (2021). https://doi.org:10.1016/j.nicl.2021.102873

Figure legends

Figure 1. Workflow of cerebrospinal fluid-based spatial statistics.

(A) Pseudo-T2 map was generated using free water map and cFA map. equation (1), GM fraction = 1- CSF fraction - WM fraction; equation (2), pseudo-T2 = CSF fraction*2 + GM fraction. (B) CSF was segmented and parcellated into ventricles, cisterns, sulci, and their subregions in native space. (C) Pseudo-diffusivity was calculated using low b-value dMRI and parcellated using atlas created in B.

GM, gray matter; CSF, cerebrospinal fluid; WM, white matter; FW, free water; cFA, free water corrected fractional anisotropy; dMRI, diffusion magnetic resonance imaging.

Figure 2. The differences of the cerebrospinal fluid pseudo-diffusivity in the combined ventricles, sulci, and cisterns.

Parkinson's disease patients showed significant decreased cerebrospinal fluid pseudo-diffusivity in the combined ventricles (A) and sulci (B), but not in the cistern (C). P value by general linear model, with age, sex, and cerebrospinal fluid volume include as covariates of no interest.

Figure 3. The relationship between cerebrospinal fluid pseudo-diffusivity and the integrity of locus coeruleus.

Differential analysis of the CNR_{LC} was performed via a general linear model, with age and sex as covariates (A). Partial correlation analysis was applied to examine the association between CNR_{LC} and pseudo-diffusivities in the combined ventricles and sulci, controlling for age, sex, and cerebrospinal fluid volume as covariates (B, C).

PD, Parkinson's disease; CSF, cerebrospinal fluid; CNR_{LC}, contrast-to-noise ratio of locus coeruleus.

Tables

Table 1. Demographic characteristics.

	Healthy control (n =48)	Parkinson's disease (n=44)	P
Sex (M/F)	27/21	25/19	0.957
Age (Year)	60.76±5.2	62.65±6.55	0.127
Educational level (Year)	7.22±3.55	6.45±4.62	0.374
Disease duration (Year)	-	3.91±2.49	-
LEDD	-	239.75±219.8	-
UPDRS-I	0.83±0.86	1.57±1.69	0.009
UPDRS-II	0.92±1.58	7.89±4.64	<0.001
UPDRS-III	1±1.15	22.14±12.14	<0.001
Axial	-	4±2.74	-
Tremor	-	3.73±3.19	-
Rigidity	-	4.43±3.79	-
Bradykinesia	-	9.82±6.25	-
Hoehn & Yahr	-	2.1±0.45	-
MMSE	26.19±3.16	25.14±4.81	0.215
RBDQ-HK	14.9±9.57	20.9±14.51	0.022
SCOPA-AUT	4.77±3.73	10.88±5.68	<0.001

P value by chi-square or Student's t test. Frequencies were used to describe the categorical variable. Mean and SD were used to describe the continuous variable.

LEDD, levodopa equivalent daily dose; UPDRS, Unified Parkinson's Disease Rating Scale; MMSE, Mini-mental state examination; RBDQ-HK, Rapid Eye Movement Sleep Behavior Disorder Questionnaire—Chinese University of Hong Kong version; SCOPA-AUT, Scales for Outcomes in Parkinson's Disease—Autonomic.

Table 2. Differences in CSF pseudo-diffusivity among ventricles, sulci, and cisterns between groups.

Regions	Healthy control	Parkinson's disease	P (FDR corrected)
Left lateral ventricle	0.00321±0.00071	0.00259±0.00061	<0.001
Right lateral ventricle	0.00312±0.00071	0.00258±0.00065	0.001
Third ventricle	0.00855±0.00205	0.00768±0.00193	0.100
Fourth ventricle	0.00666±0.00174	0.00609±0.0017	0.129
Left central sulcus	0.00211±0.00063	0.00155±0.00046	<0.001
Left intraparietal sulcus	0.00173±0.00057	0.00143±0.00046	0.008
Left postcentral sulcus	0.00188±0.00056	0.00139±0.00044	<0.001
Left precentral sulcus	0.00222±0.00067	0.00165±0.00056	<0.001
Left superior temporal sulcus	0.00285±0.00096	0.00238±0.001	0.004
Left Sylvian fissure	0.0065±0.00135	0.00619±0.00142	0.312
Right central sulcus	0.00206±0.00063	0.00158±0.00043	<0.001
Right intraparietal sulcus	0.00177±0.00052	0.00142±0.00048	0.002
Right postcentral sulcus	0.00198±0.00063	0.00149±0.00052	0.001
Right precentral sulcus	0.00223±0.00067	0.00169±0.00055	<0.001
Right superior temporal sulcus	0.00258±0.00097	0.00213±0.00094	0.011
Right Sylvian fissure	0.00736±0.0014	0.00699±0.0016	0.377
Superior longitudinal fissure (anterior part)	0.00252±0.00075	0.00192±0.00049	0.001
Superior longitudinal fissure (posterior part)	0.00228±0.00087	0.00166±0.00041	0.001
Suprasellar cistern	0.01149±0.00105	0.01184±0.00138	0.369
Premedullary cistern	0.01506±0.00234	0.01479±0.00198	0.924
Prepontine cistern	0.0128±0.00137	0.01248±0.00171	0.200
Quadrigeminal cistern	0.00617±0.00105	0.00589±0.00131	0.181
Left ambient cistern	0.01033±0.00158	0.00966±0.00168	0.086
Left cerebellopontine angle cistern	0.00725±0.00167	0.00685±0.00182	0.964
Left crural cistern	0.01119±0.00197	0.01071±0.00187	0.030
Right ambient cistern	0.01009±0.00137	0.00961±0.00187	0.312
Right cerebellopontine angle cistern	0.00699±0.00172	0.00651±0.00196	0.924
Right crural cistern	0.01029±0.00156	0.01014±0.00187	0.205

P value by general linear model, with age, sex, and cerebrospinal fluid volume include as covariates of no interest.

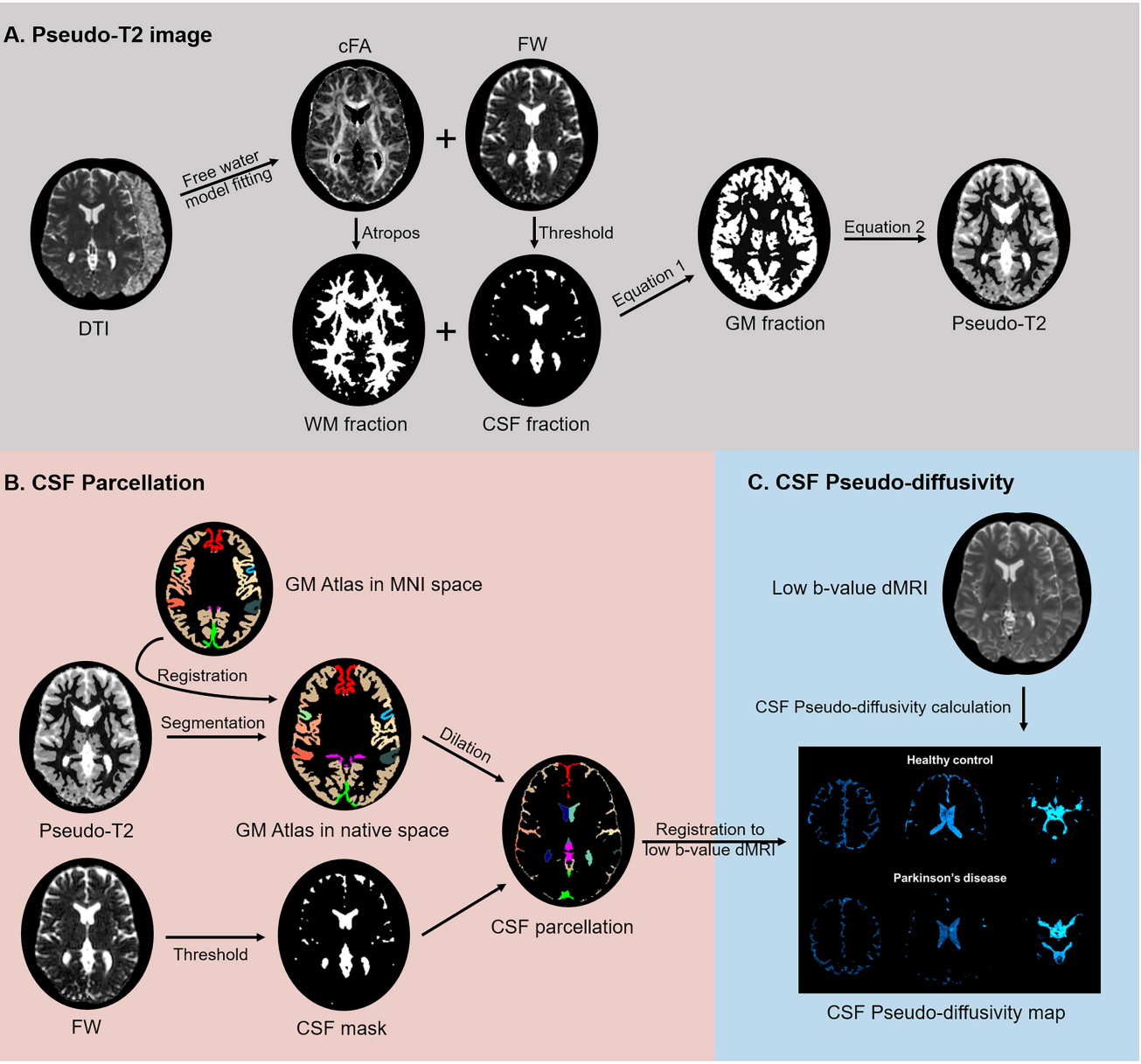
A. Pseudo-T2 image
cFA
FW
Free water model fitting
DTI
Atropos
Threshold
WM fraction
CSF fraction
Equation 1
GM fraction
Equation 2
Pseudo-T2
B. CSF Parcellation
GM Atlas in MNI space
Registration
Segmentation
Pseudo-T2
GM Atlas in native space
Dilation
CSF parcellation
Threshold
FW
CSF mask
C. CSF Pseudo-diffusivity
Low b-value dMRI
CSF Pseudo-diffusivity calculation
Registration to low b-value dMRI
Healthy control
Parkinson's disease
CSF Pseudo-diffusivity map

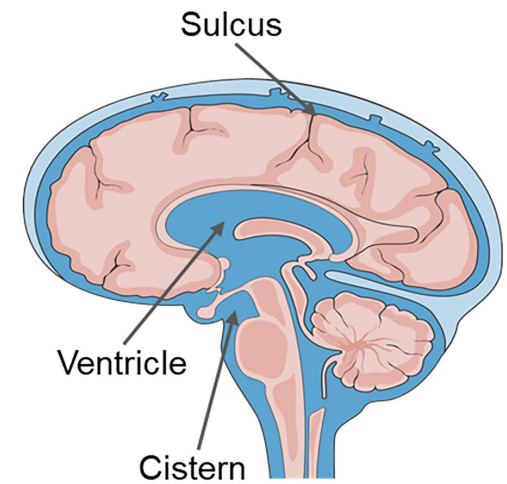
Sulcus
Ventricle
Cistern

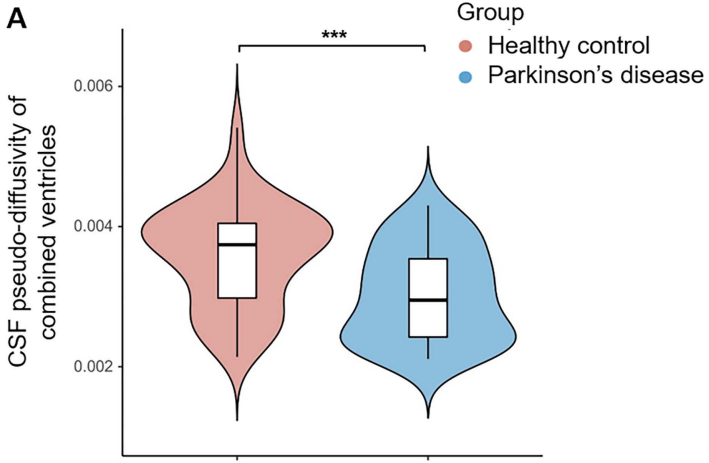
A
Group
Healthy control
Parkinson's disease
***
CSF pseudo-diffusivity of combined ventricles
0.006
0.004
0.002

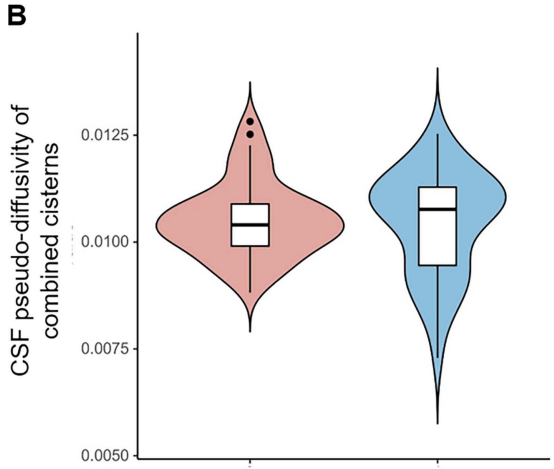
B
CSF pseudo-diffusivity of combined cisterns
0.0125
0.0100
0.0075
0.0050

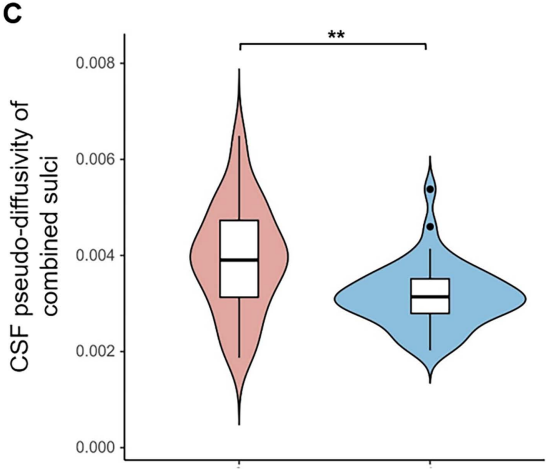
C
**
CSF pseudo-diffusivity of combined sulci
0.008
0.006
0.004
0.002
0.000

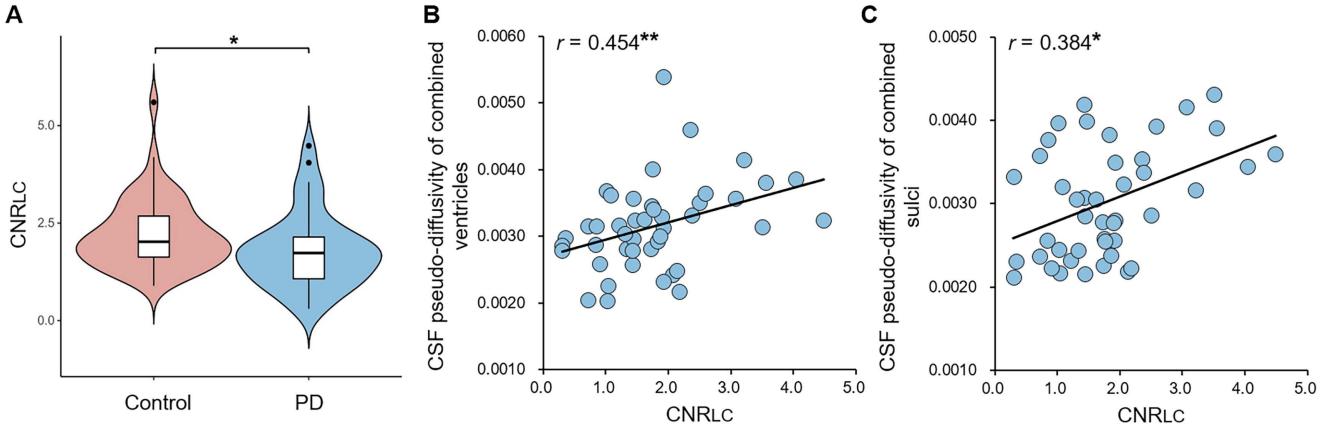
A
*
CNRLC
5.0
2.5
0.0
Control
PD
B
r = 0.454**
CSF pseudo-diffusivity of combined ventricles
0.0060
0.0050
0.0040
0.0030
0.0020
0.0010
0.0
1.0
2.0
3.0
4.0
5.0
CNRLC
C
r = 0.384*
CSF pseudo-diffusivity of combined sulci
0.0050
0.0040
0.0030
0.0020
0.0010
0.0
1.0
2.0
3.0
4.0
5.0
CNRLC